

The feature of shadow images and observed luminosity of the Bardeen black hole surrounded by different accretions

Ke-Jian He,^a Sen Guo,^b Shuang-Cheng Tan,^a Guo-Ping Li^c

^a*College Of Physics, Chongqing University, Chongqing 401331, China*

^b*Guangxi Key Laboratory for Relativistic Astrophysics, School of Physical Science and Technology, Guangxi University, Nanning 530004, China*

^c*Physics and Space College, China West Normal University, Nanchong 637000, China*

E-mail: kjhe94@163.com, sguophys@126.com, 445568834@qq.com,
gpliphs@yeah.net

ABSTRACT: By exploring the photon motion in the region near the Bardeen black hole, the shadow and luminosity of the black hole surrounded by different accretions are studied in this paper. We analyzed the changes in shadow imaging and observation luminosity when the relevant physical parameters are changed. In the static and infalling spherical accretion, although the radius of the shadow and the position of the photon spheres do not change in the two models, the observation intensity of the black hole with infalling accretion is significantly lower than that of the static accretion. In particular, in the case of the thin disk accretion, we study the contribution of the photon rings, lensing rings and direct emission to the total observed flux. The result shows that the observed brightness of black holes is mainly determined by direct emission. Furthermore, in the different forms of the emission modes, the lensing ring will provide a small part of the observation flux, while the photon ring can provide a negligible observation flux. After that, we compare our results with the Schwarzschild black hole, we find that the existence or change of the parameter g will greatly affect the imaging and observation intensity of black hole shadow. Hence, the parameter g change the spacetime structure which affects the photon sphere, the deflection angle and the observations of black hole shadows.

Contents

1	Introduction	1
2	Null geodesic in the Bardeen space-time	3
3	Image of the Bardeen black hole with spherical accretion	5
3.1	The Bardeen black hole surrounded by static spherical accretion	6
3.2	The Bardeen black hole surrounded by infalling spherical accretion	7
4	The Bardeen black hole surrounded by thin disk accretion	9
4.1	The behavior of the trajectories of light rays	9
4.2	Transfer functions	10
4.3	The observational appearance of Bardeen black hole surrounded by a thin disk accretion	12
5	Conclusions and discussions	14

1 Introduction

Since the concept of black hole was put forward, people have been trying to find this mysterious physical object in the universe. In particular, the first image of supermassive black holes at the center of M87 galaxy, which was captured by the Event Horizon Telescope Collaboration (EHT), is strong proof of the existence of the black hole[1–6]. It has been observed that the dark area appears in the background of a bright ring in the image, and this black area is called the shadow of the black hole. It is commonly known that the real astrophysical black holes in galaxies are surrounded by the accretion matter, which makes it possible to indirectly observation of the black hole. Therefore, the observational properties of the black hole can be reflected by the accretion near the black hole.

A lot of studies focused on black hole shadow and its observation[7–27], and there are also some interesting ideal models. Although the accretion current around a black hole is usually not spherically symmetric in reality, the simplified ideal spherical model can provide strong support for the characteristics of black hole observation. It is generally accepted that the shape of the black hole shadow is circular geometry for static spherically symmetric black holes, and the image of the black hole surrounded by a geometrically and optically accretion disk has been studied[28, 29]. Taking into account the model in which the black hole surrounded by the spherical accretion, the results show that the shape and size of the shadow are geometric characteristics of space-time and has nothing to do with the details of the accretion process, but the observed luminosity is affected by the state of the accretion model [30–33]. In addition, Ref.[34] analyzed the observational peculiarity

of the black hole observed by the distant observer, when an optically and geometrically thin disk accretion is located on the equatorial plane of the black hole. They divide the trajectories of light rays into direct, lensed and photon ring ones, and proposed that the observed characteristics of black holes are dominated by the direct case. Furthermore, they also found that the size of the black center region depends on the specific emission mode, although the size of the final observed features is similar. After that, there is some progress in the study of shadow, lens ring and photon ring of other black hole models[35, 36].

With the deepening of the study of black hole shadow, many studies also pay more attention to the observation of black hole shadow, because it will bring new insights and development to the study of black hole. In this paper, we focus on the observational images and luminosity of the Bardeen black hole surrounded by different accretion models. The first regular black hole without singularity was proposed by Bardeen[37]. Since then, the research of regular black holes has aroused people's interest. Furthermore, more regular black hole models have been established, and the related physical properties have been widely studied.[38–49]. Therefore, it is necessary to study the influence of the relevant state parameters on the shadow image and observation characteristics in the Bardeen black hole. Here, we mainly consider the static, infalling spherical accretion and the geometrically thin and optically thin disk accretion, and compare the results of the three models. For the spherically symmetric accretion, we found that the change of the state parameter g will affect the shadow radius and the position of the photon sphere of the black hole, but the state of the accretion matter will not. However, for an observer at infinity, the details of the accretion have a significant effect on the observation intensity. Specifically, the Bardeen black hole surrounded by infalling spherically symmetric accretion has a darker shadow area, and the difference of the observed luminosity of the black hole image with the change of parameter g is more obvious. The reason can be explained by the Doppler effect. For the thin disk accretion, the shadow, lens ring and photon ring appear near the black hole. Due to the extreme demagnetization, the remote observer can not obtain the observation flux provided by the photon ring. Hence, the intensity of observation is provided by the direct image from accretion, and the lens ring also contributes, but only a small part. In addition, different emission profiles of the accretion will also directly affect the observed specific intensity.

The paper is organized as follows. In section 2, we have studied the associated trajectories of the light ray near the Bardeen black hole, and the radius of photon sphere and shadow of the black hole under different state parameters g is obtained. In section 3, we analyze the shadow image and luminosity of the black hole surrounded by the different states of spherical accretion. In section 4, we consider thin disk emission near the black hole, and compare the observational appearance with the different emission profiles. Finally, we discuss our results and conclusions in section 5. In this paper, we use the units $G = c = 1$.

2 Null geodesic in the Bardeen space-time

We would like to consider the spherically symmetric static metric of the black hole, and the Regular black hole metric was introduced by Bardeen as follows[37],

$$ds^2 = -A(r)dt^2 + B(r)dr^2 + C(r)(d\theta^2 + \sin^2\theta d\varphi^2), \quad (2.1)$$

with

$$A(r) = 1 - \frac{2Mr^2}{(g^2 + r^2)^{3/2}}, \quad B(r) = \frac{1}{A(r)}, \quad C(r) = r^2. \quad (2.2)$$

Here, M is the mass of the black hole and g is the monopole charge of the non-linear self gravitating magnetic field. It may be noted that the space-time structure of Bardeen black hole recovers to the Schwarzschild space-time for $g = 0$, and we have regular values in all points of the space-time for $g \neq 0$. As mentioned in [50], the metric function $f(r)$ on behaves asymptotically i.e at $r \rightarrow \infty$. Thus, the metric function can be approximated as

$$A(r) \sim 1 - \frac{2M}{r} + \frac{3g^2M}{r^3} + \mathcal{O}\left(\frac{1}{r^5}\right). \quad (2.3)$$

In addition, the above black hole metric reduces to de-Sitter space-time for $r \rightarrow 0$, which is

$$A(r) \sim 1 - \frac{2Mr^2}{g^3}. \quad (2.4)$$

Solving equation $A(r) = 0$, we can get the horizon of the Bardeen black hole. There would be the inner horizon and the outer one as event horizon (r_h) when $g < \frac{4\sqrt{3}}{9}M$, and the inner and outer horizons will be closely overlapped when $g = \frac{4\sqrt{3}}{9}M$. However, for the case $g > \frac{4\sqrt{3}}{9}M$, there is no horizon and we do not consider this situation [50].

When the light ray passes from the vicinity of a massive object it is deflected duo to the interaction between light and gravitational field of the massive object. Let us now turn to the particle motion around the black hole. In doing so, we can use the Euler-Lagrange equation, and for the test, the particle is photon it reads as

$$\frac{d}{d\lambda} \left(\frac{\partial \mathcal{S}}{\partial \dot{x}^\mu} \right) = \frac{\partial \mathcal{S}}{\partial x^\mu}, \quad (2.5)$$

where λ and \dot{x}^μ are the affine parameter and four-velocity of the lights, respectively. For the metric function (2.1), the Lagrangian \mathcal{S} can be expressed as

$$\mathcal{S} = \frac{1}{2} g_{\mu\nu} \dot{x}^\mu \dot{x}^\nu = \frac{1}{2} \left(-A(r)\dot{t}^2 + B(r)\dot{r}^2 + C(r) \left(\dot{\theta}^2 + \sin^2\theta \dot{\varphi}^2 \right) \right). \quad (2.6)$$

Since it is a spherically symmetric space-time, for simplicity, we can only discuss the motion of photons on the equatorial plane[9, 51, 52]. Hence, we have the restrictive conditions $\theta = \frac{\pi}{2}$ and $\dot{\theta} = 0$. Duo to the t and θ coordinates can not explicitly determine the coefficient of the metric equation, there are two conserved quantities E and L (representing energy and angular momentum respectively). That is

$$E = -\frac{\partial \mathcal{S}}{\partial \dot{t}} = A(r)\dot{t}, \quad L = \frac{\partial \mathcal{S}}{\partial \dot{\varphi}} = r^2\dot{\varphi}. \quad (2.7)$$

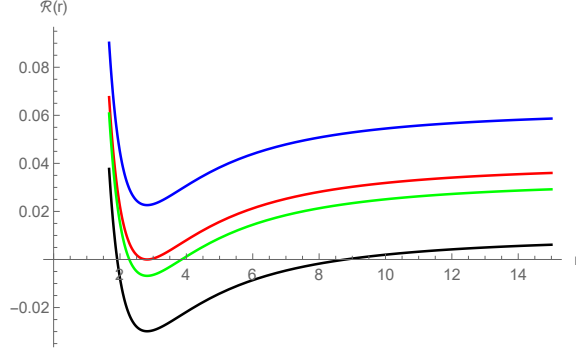


Figure 1. The relationship between $\mathcal{R}(r)$ and impact parameter b with $M = 1$, $g = 0.45$. Here, $b = 4.0$ (blue line), $b = 5.00837$ (red line), $b = 5.50$ (green line) and $b = 10$ (black line)

For null geodesic, we have $g_{\mu\nu}\dot{x}^\mu\dot{x}^\nu = 0$. Therefore, we can obtain that

$$\dot{r}^2 = E^2 - \frac{L^2}{r^2}A(r). \quad (2.8)$$

Then, the motion equation of photons can be read as

$$\mathcal{R}(r) = \frac{1}{b^2} - \frac{A(r)}{r^2}, \quad (2.9)$$

in which, b is the impact parameter and $b = L/E$. We can give the image of $\mathcal{R}(r)$ corresponding to different values of the impact parameter b , as shown in Figure 1.

As can be seen from Figure 1, when the impact parameter $b = b_p \sim 5.00837$, the image of $\mathcal{R}(r)$ has only one intersection with the horizontal axis (red line). In other words, the photon is in the critical state of falling into or escaping from the black hole, and will move to the circular orbit of $r = r_p$ near the black hole. The surface corresponding to r_p is called the photon sphere. On the other hand, the condition that a black hole can capture the light ray should be satisfied $\dot{r} = 0$ and $\ddot{r} = 0$, which means[32]

$$r_p^2 - b_p^2 A(r) = 0, \quad 2b_p^2 A(r)^2 - r_p^3 A'(r) = 0. \quad (2.10)$$

For the distant observer, b_p is the value of the radius of the shadow that can be seen. For the different values of g , we can get the different numerical results of the radius r_p , the radius of the shadow b_p and the event horizon r_h where $M = 1$, and listed in Table 1.

Table 1. The value of the relevant physical quantity for different state parameter g which $M = 1$.

	$g = 0.1$	$g = 0.2$	$g = 0.3$	$g = 0.4$	$g = 0.475$	$g = 0.6$	$g = 0.7$	$g = 0.7698003$
r_p	2.99164	2.96617	2.9224	2.85798	2.7937	2.64674	2.47495	2.30118
b_p	5.18747	5.16108	5.11594	5.05508	4.98508	4.83975	4.67719	4.52406
r_h	1.99247	1.96946	1.92962	1.87022	1.80981	1.66546	1.47436	1.08903

From Table 1, we can see that the radius r_p , the radius of the shadow b_p and the event horizon r_h all show a decreasing trend, as the increase of parameter g . With the help of introducing parameter $u_0 = 1/r$, we can rewrite the motion equation of photons, and use

it to depict the trajectory of light ray. Thus, we can get

$$\mathcal{V}(u_0) = \frac{du_0}{d\varphi} = \sqrt{\frac{1}{b^2} - u_0^2 \left(1 - \frac{2M}{u_0^2 \left(g^2 + \frac{1}{u_0^2} \right)^{3/2}} \right)}. \quad (2.11)$$

It is worth noting that the geometry of geodesics depends entirely on the above equation. In the case of $b < b_p$, the light ray is always trapped by the black hole and cannot reach infinity distance. In the case of $b > b_p$, the light ray will be deflected at the radial position u_0 when $\mathcal{V}(u_0) = 0$, and then move away from the black hole reach infinity distance. When $b = b_p$, the photon will rotate around the black hole in the photon sphere. In the following sections, we further study the shadow of black holes surrounded by various profiles of accretions.

3 Image of the Bardeen black hole with spherical accretion

With the help of equation (2.11), we know that the trajectory of a light ray is changed as the change of the value of the state parameter g and impact parameter b . Therefore, we simply describe the path of light rays under the relevant physical parameters, as shown in Figure 2. In Figure 2, we take $g = 0.475$ (On the left) and $g = 0.7698003$ (On the right) as

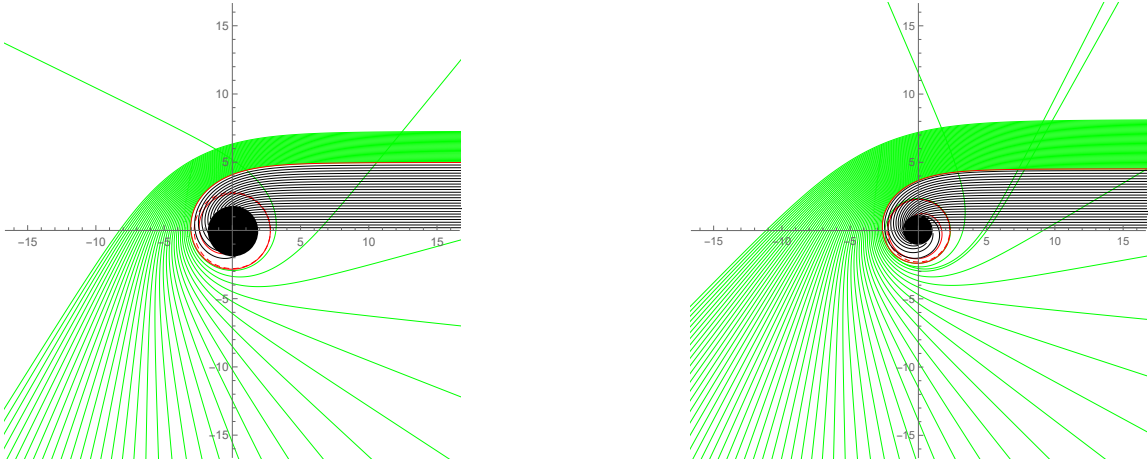


Figure 2. The trajectory of the light ray for the different value of g in the polar coordinates (r, φ) with $M = 1$, and the black hole is shown as a black disk.

two examples. Here, the red lines, green lines and black lines correspond to $b = b_p$, $b > b_p$ and $b < b_p$, respectively. It is obvious that the radius of the photon sphere r_p decreases when the parameter g increases, which is consistent with the cases in Table 1. Compare the results in Figure 2, we find that when the value of g is larger, the deflection of a light ray at the photon sphere is larger and the light ray density is higher. For the distant observer, the radius of black hole shadow and photon sphere decrease with the increase of g , but the luminosity around the black hole will increase. Therefore, we are in a position to study the image of the black hole with the spherical accretion. In this section, we mainly consider two simple relativistic spherical accretion models, that is, the static spherical accretion and the infalling spherical accretion.

3.1 The Bardeen black hole surrounded by static spherical accretion

In this section, we consider the static spherical accretion. We can integrate the specific emissivity along the photon path γ_i to get the specific intensity observed by the observer \mathcal{I}_{obs} (usually measured in $\text{ergs}^{-1}\text{cm}^{-2}\text{str}^{-1}\text{Hz}^{-1}$). That is [7, 32]

$$\mathcal{I}_{obs}(\nu_0) = \int_{\gamma_i} \mathcal{G}^3 j(\nu_e) dl_{prop}, \quad (3.1)$$

where

$$\mathcal{G} = \frac{\nu_0}{\nu_e}. \quad (3.2)$$

It is worth mentioning that we focus on the measured in the rest-frame of the emitter. Here, \mathcal{G} is the redshift factor, ν_e is the photon frequency at the emitter, $j(\nu_e)$ is the emissivity per-unit volume at the emitter, and dl_{prop} is the infinitesimal proper length. In addition, ν_0 is the observed photon frequency. In $4-D$ static spherically symmetric space-time(2.1), the redshift factor $\mathcal{G} = A(r)^{\frac{1}{2}}$. For the specific emissivity $j(\nu_e)$, we consider that the emission is monochromatic with the emission frequency ν_f , and the emission radial profile is $1/r^2$, that is,

$$j(\nu_e) \sim \frac{\delta(\nu_e - \nu_f)}{r^2}, \quad (3.3)$$

where δ is the delta function. Form the equation (2.1), we can obtain the proper length is

$$dl_{prop} = \sqrt{\frac{1}{A(r)} + r^2 \left(\frac{d\varphi}{dr}\right)^2} dr. \quad (3.4)$$

So, the expression for the specific intensity observed by the distance observer (3.1) can be rewritten as

$$\mathcal{I}_{obs}(\nu_0) = \int_{\gamma_i} \frac{(A(r))^{3/2}}{r^2} \sqrt{\frac{1}{A(r)} + r^2 \left(\frac{d\varphi}{dr}\right)^2} dr. \quad (3.5)$$

From the above equation, the change of relevant physical quantity will directly affect the specific intensity observed by a distant observer. Therefore, we take $g = 0$, $g = 0.475$ and $g = 0.7698003$ as examples, the image of the change of the observed intensity with the different value of b is given in Figure 3.

It is clear that the observation intensity increases slowly with the increase of b , then increases rapidly near the photon sphere, and finally reaches the peak at the position of the photon sphere. However, the observation intensity decreases with the increase of b after reaching the peak and finally tends to a minimum value. In addition, the value of g is changed, the variation characteristics of observation intensity are similar. However, the larger value of b , the stronger specific intensity observed. When $g = 0$ (the Schwarzschild space-time), the peak of observation intensity is obviously smaller than that when $g \neq 0$. In other words, the observational intensity of the Bardeen space-time is stronger than that of the Schwarzschild space-time. Then, the 2-dimensional image of the shadows is shown in Figure 4.

From Figure 4, there is a bright ring with the strongest luminosity, which is in the position of the photon sphere. Moreover, the inner region of the photon sphere is not

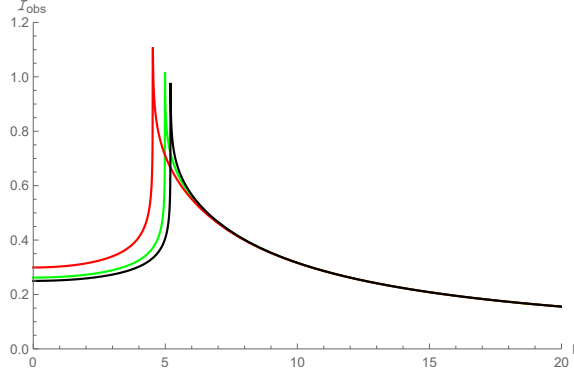


Figure 3. The observed specific intensity of the black hole is surrounded by the static spherical accretion, in which the black line, green line and red line correspond to $g = 0$, $g = 0.475$ and $g = 0.7698003$. Here, we set $M = 1$.

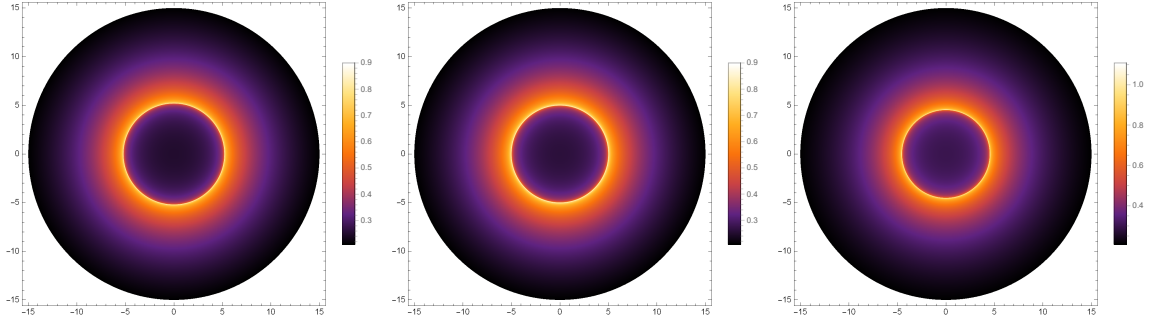


Figure 4. Image of the black hole shadow with the static spherical accretion for the different value of g , in which $g = 0$ (left panel), $g = 0.475$ (mid panel) and $g = 0.7698003$ (right panel).

completely black, and there is small luminosity near the photon sphere, due to the tiny fraction of the radiation that can escape from the black hole. Obviously, the maximum luminosity of the shadow image is enhanced with the increase of parameter g , but the size of black hole shadow decrease with the parameter g .

3.2 The Bardeen black hole surrounded by infalling spherical accretion

Next, we will investigate the infalling spherical accretion around the Bardeen black hole where the radiating gas moves towards the black hole along the radial direction. In fact, the infalling spherical accretion is closer to the real situation than the static spherical accretion. In this case, we still use the equation (3.5) to study the shadow, but we need to pay attention to that the redshift factor of static and the infalling accretion are different. Due to the redshift factor for the infalling accretion is related to the velocity of the accretion. For the infalling spherical accretion, the corresponding redshift factor is

$$\mathcal{G}_i = \frac{\mathcal{K}_\rho u_0^\rho}{\mathcal{K}_\sigma u_e^\sigma}, \quad \mathcal{K}^\mu = \dot{x}^\mu, \quad (3.6)$$

where \mathcal{K}^μ is the four-velocity of the photon and $u_0^\mu = (1, 0, 0, 0)$ is the four-velocity of the static observer. Moreover, the four-velocity of the infalling accretion correspond to u_e^μ ,

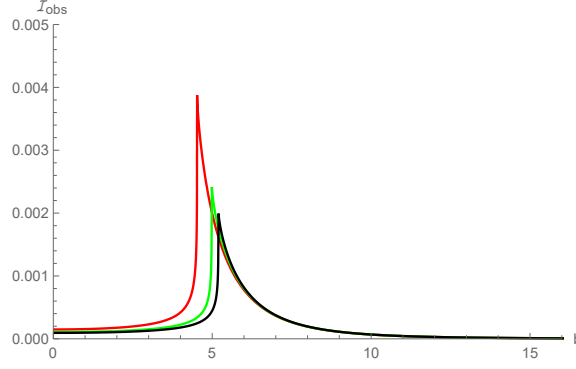


Figure 5. The observed specific intensity of the black hole is surrounded by the infalling spherical accretion, in which the black line, green line and red line correspond to $g = 0$, $g = 0.475$ and $g = 0.7698003$. Here, we set $M = 1$.

which is

$$u_e^t = A(r)^{-1}, \quad u_e^r = -\sqrt{\frac{1-A(r)}{A(r)B(r)}}, \quad u_e^\theta = u_e^\varphi = 0. \quad (3.7)$$

Here, \mathcal{K}_t is a constant of motion, and \mathcal{K}_r can be obtain by the equation $\mathcal{K}_\mu \mathcal{K}^\mu = 0$ for the photon. That is

$$\mathcal{K}_t = \frac{1}{b}, \quad \frac{\mathcal{K}_r}{\mathcal{K}_t} = \pm \sqrt{B(r) \left(\frac{1}{A(r)} - \frac{b^2}{r^2} \right)}, \quad (3.8)$$

where the sign $+$ or $-$ corresponds to the case that the photon approaches to or goes away from the black hole. Hence, the redshift factor of the infalling accretion is

$$\mathcal{G}_i = \left(u_e^t + \left(\frac{\mathcal{K}_r}{\mathcal{K}_t} \right) u_e^r \right)^{-1}. \quad (3.9)$$

In the other hand, the form of the proper distance should be rewritten as

$$dl_{prop} = \mathcal{K}_\mu u_e^\mu d\lambda = \frac{\mathcal{K}_t}{\mathcal{G}_i |\mathcal{K}_r|} dr. \quad (3.10)$$

In addition, we also consider that the specific emissivity has the same form as in the equation (3.3). Lastly, we obtain the observed flux in the case with infalling spherical accretion

$$\mathcal{I}_{obs} \propto \int_{\gamma_i} \frac{\mathcal{G}_i^3 \mathcal{K}_t dr}{r^2 |\mathcal{K}_r|}. \quad (3.11)$$

Based on the above equation, we also can investigate the shadow and luminosity of the regular black hole, surrounded by the infalling spherical accretion. Similarly, we also give the image of luminosity distribution under different state parameters, which is shown in Figure 5.

We find that the maximum observed intensity still at the position of the photon sphere ($b \sim b_p$). In addition, the observed intensity increases with the increase of b in the region of $b < b_p$, but decreases with the increase of b in the region $b > b_p$. These characteristics

are consistent with the case of static accretion. However, the peak value of the observed intensity is much smaller than that of the static accretion, which shows that the shadow image of the infalling spherical accretion is darker than that of the static case. On the other hand, the observation intensity also increases with the increase of parameter g , but the increased intensity of infalling accretion is greater than that of the static case, the difference of peak value is more obvious. The two-dimensional image of the intensity is also shown in Figure 6.

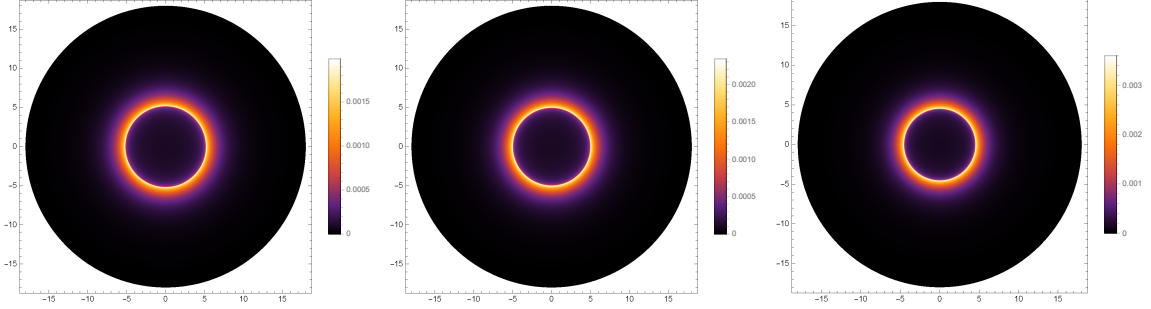


Figure 6. Image of the black hole shadow with the infalling spherical accretion for the different value of g , in which $g = 0.475$ (left panel) and $g = 0.7698003$ (right panel).

The central region inside the photon sphere in Figure 6 is indeed darker than the corresponding region in Figure 4. Moreover, the intensity of the bright ring is far less than that of static accretion. The difference between the two spherical accretions models is due to the Doppler effect. Comparing with static spherical accretion, we also find that the radii of the shadow and the position of the photon sphere remain unchanged. In other words, the behavior of the accretion material will affect the observation intensity, but will not affect the radius of the shadow and the position of the photon sphere.

4 The Bardeen black hole surrounded by thin disk accretion

4.1 The behavior of the trajectories of light rays

In this section, we are going to consider a thin accretion disk around the Bardeen black hole on the equatorial plane, which is the optically and geometrically thin disks for simplicity. The light ray trajectories near the black hole are the important basis for studying the observational appearance of a black hole. As in Ref.[34], to distinguish the trajectories of light rays, they put forward the total number of orbits and defined it as

$$n(b) = \frac{\varphi}{2\pi}, \quad (4.1)$$

which is a function of impact parameter b . By equation (4.1), they divide trajectories into direct, lensed and photon ring ones. In addition, they found that there are not only the photon rings but also lens rings near the shadow of black hole. Specifically, when $n(b) < 3/4$, the light ray trajectories will intersect the equatorial plane only once, and it corresponds to the direct emissions; when $3/4 < n(b) < 5/4$, the light ray crossing the

equatorial plane at least twice, and it corresponds to the lensing rings; when $n(b) > 5/4$, will intersect the equatorial plane at least three times, and it corresponds to the photon rings. Here, we still use $g = 0$, $g = 0.475$ and $g = 0.7698003$ as examples, and plot the relationship between the total number of orbits $n(b)$ and impact parameter b in the Bardeen space-time, as shown in Figure 7. We find that the parameter g changes, the same value of

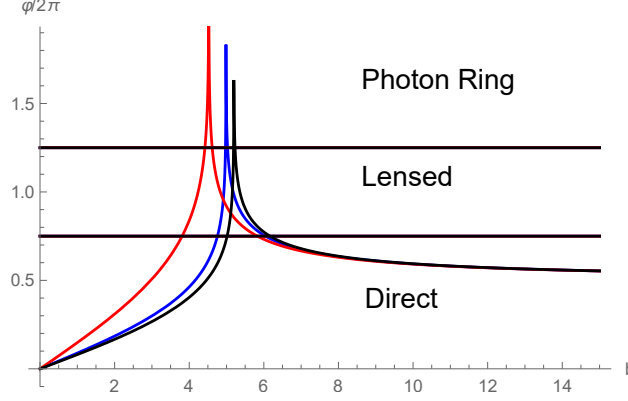


Figure 7. Behavior of photons in Bardeen black hole as a function of impact parameter b . The colors correspond to $g = 0$ (black), $g = 0.475$ (blue), and $g = 0.7698003$ (red), respectively. Here, we set $M = 1$.

b may correspond to different regions. When $g = 0.7698003$, the region of photon rings in Bardeen space-time is obviously larger than that in Schwarzschild space-time ($g = 0$). Then, the parameter b increases to a large enough value, the light ray trajectories are the direct emissions no matter what the value of g is. In other words, the parameter g and b will affect the observed characteristics of the Bardeen black hole. In order to more clearly distinguish the distribution of photon trajectories near the black hole, we take $g = 0.7698003$ as an example, as shown in Figure 8.

4.2 Transfer functions

In this section, we will investigate the observed specific intensity of the Bardeen black hole, surrounded by the thin disk accretion. We consider that a distance static observer is located in the north pole, and the thin disk accretion at the equatorial plane of the black hole. Moreover, the lights emitted from the thin disk accretion is isotropically for the static observer. In our case, the specific intensity and frequency of the emission are expressed as $I_\nu^{em}(r)$ and ν_{em} , and the observed specific intensity and frequency are defined as $I_\nu^{obs}(r)$ and ν_{obs} . Considering $\frac{I_\nu^{em}}{\nu_e^3}$ is conserved along a ray from the Liouville theorem, that is, there is a correlation between the observed specific intensity and the emissivity specific intensity [35]

$$I_\nu^{obs} = (A(r))^{3/2} I_\nu^{em}(r). \quad (4.2)$$

Thus, integrating for the full frequency, we can get the total observation and emitted intensity, which is

$$I_O = \int I_\nu^{obs}(r) d\nu'_{obs} = \int (A(r))^2 I_\nu^{em} d\nu_{em} = (A(r))^2 I_\nu^{em}(r), \quad I_E = \int I_\nu^{em}(r) d\nu_{em}. \quad (4.3)$$

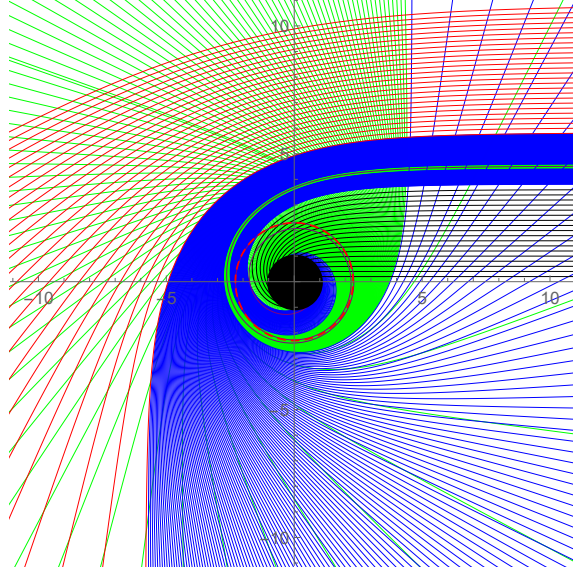


Figure 8. The selection of associated photon trajectories in the polar coordinates (b, φ) , in which the red lines, blue lines and green lines correspond to direct, lensing, and photon ring bands. Here, the spacing in impact parameter is $1/10$, $1/100$, and $1/1000$ in the direct, lensed and photon ring, respectively, and we set $M = 1$, $g = 0.7698003$.

It is worth mentioning that we only consider the intensity of light emitted only from the accretion disk, and we do not consider the absorption or reflection of light and other factors. Therefore, when the light ray trajectories pass through the accretion disk on the equatorial disk, a certain luminosity will be obtained, and transmitted to the observer at infinity. As discussed earlier, the different values for the number of orbits $n(b)$ defined the number of times the ray path pass through the equatorial plane of the black hole. In the case of $3/4 < n(b) < 5/4$, after the first intersection with the thin disk, the light ray will bend around the black hole and intersect with the back of the thin disk. In this way, the light ray will pass through the thin disk twice. For $n(b) > 5/4$, due to the light ray is more curved around the black hole, the light passes through the back of the thin disk and then through the front of the thin disk again. That is, the light will pass through the thin disk at least three times. Hence, the sum of the intensities at each intersection is the total intensity that the observer can observe, which is

$$I_O(r) = \sum_n (A(r))^2 I_E|_{r=r_n(b)}. \quad (4.4)$$

Here, $r_n(b)$ is the transfer function, which represents the radial position of the n_{th} intersection with the thin emission disk. Therefore, the relationship between radial coordinate r and impact parameter b can be expressed by the transfer function. In addition, dr/db corresponds to the slope of the transfer function, which is called the demagnification factor, and it reflects the demagnified scale of the transfer function[34, 35]. Taking $g = 0.475$ and $g = 0.7698003$ as two examples, the graph of the transfer functions is given in Figure 9. And the relation graph of $g = 0$ (Schwarzschild space time), please refer to Ref.[34].

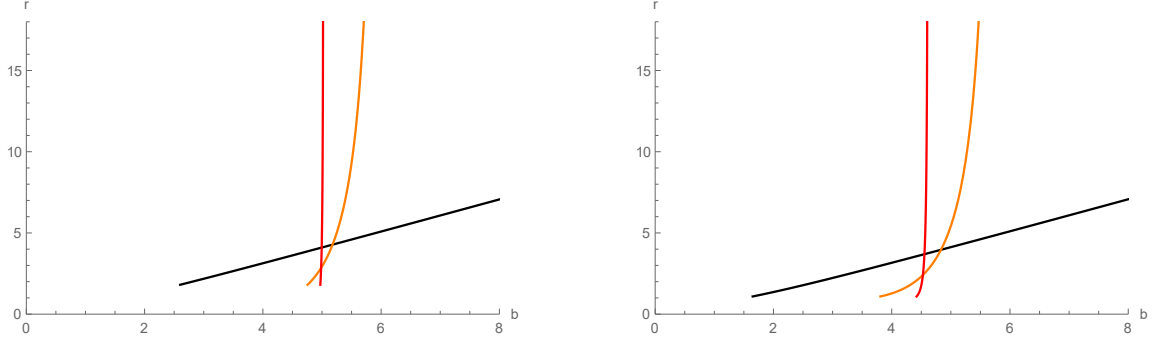


Figure 9. The relationship between The first three transfer functions $r_n(b)$ and b in the Bardeen space time, in witch $g = 0.475$ (left panel) and $g = 0.769800$ (right panel).

The black line corresponds to the first transfer function ($n = 1$), and its slope $\frac{dr}{db}|_1$ is a small value. In fact, the first transfer function corresponds to the direct image of the thin emission disk, which is the redshift of the source profile. The orange line corresponds to the second transfer function ($n = 2$), and we find that its slope $\frac{dr}{db}|_2$ is a large value. That is, the second transfer function shows a highly demagnified image on the back of the thin disk, and it corresponds to the lensing ring. The red line represents the third transfer function ($n = 3$), whose slope $\frac{dr}{db}|_3$ is close to infinity ($\frac{dr}{db}|_3 \sim \infty$). Namely, the observer will see an extremely demagnified image of the front side of the disk, and the third transfer function corresponds to the photon ring. Therefore, the luminosity provided by the photon ring and lens ring only accounts for a small proportion of the total observed flux. In particular, the image provided by the later transfer function is more demagnetized and negligible, so we only consider the first three transfer functions.

4.3 The observational appearance of Bardeen black hole surrounded by a thin disk accretion

With the help of function (4.3), we can further study the specific intensity of emission. We consider that the peak of emission intensity is in the position of the innermost stable circular orbit (r_{isco}), and there will be no emission inside the circular orbit, but there is a trend of sharp decline outside the innermost stable circular orbit. Which is

$$I_E(r1) = \begin{cases} \left(\frac{1}{r-(r_{isco}-1)}\right)^2, & r > r_{isco} \\ 0, & r < r_{isco} \end{cases} \quad (4.5)$$

Then, we assume that the position of the emission peak in the photon sphere (r_p), and the emission is a decay function of the power of third. That is

$$I_E(r2) = \begin{cases} \left(\frac{1}{r-(r_p-1)}\right)^3, & r > r_p \\ 0, & r < r_p \end{cases} \quad (4.6)$$

Finally, we consider there is the decaying gradually of the emission between the event horizon r_h and the innermost stable circular orbit r_{isco} , such as

$$I_E(r) = \begin{cases} \frac{1 - \tan^{-1}(r-5)}{1 - \tan^{-1}(r_h-5)}, & r > r_h \\ 0, & r < r_h \end{cases} \quad (4.7)$$

Now, we can take $g = 0.475$ as an example, and show the results about the intensity of the emission and observation in Figure 9. In Figure 9, the left column is the plots of different emission profiles $I_E(r)$; the middle column shows the relationship between the observed intensity $I_O(r)$ and the impact parameter b ; the right column is the density plots of observed intensities $I_O(r)$.

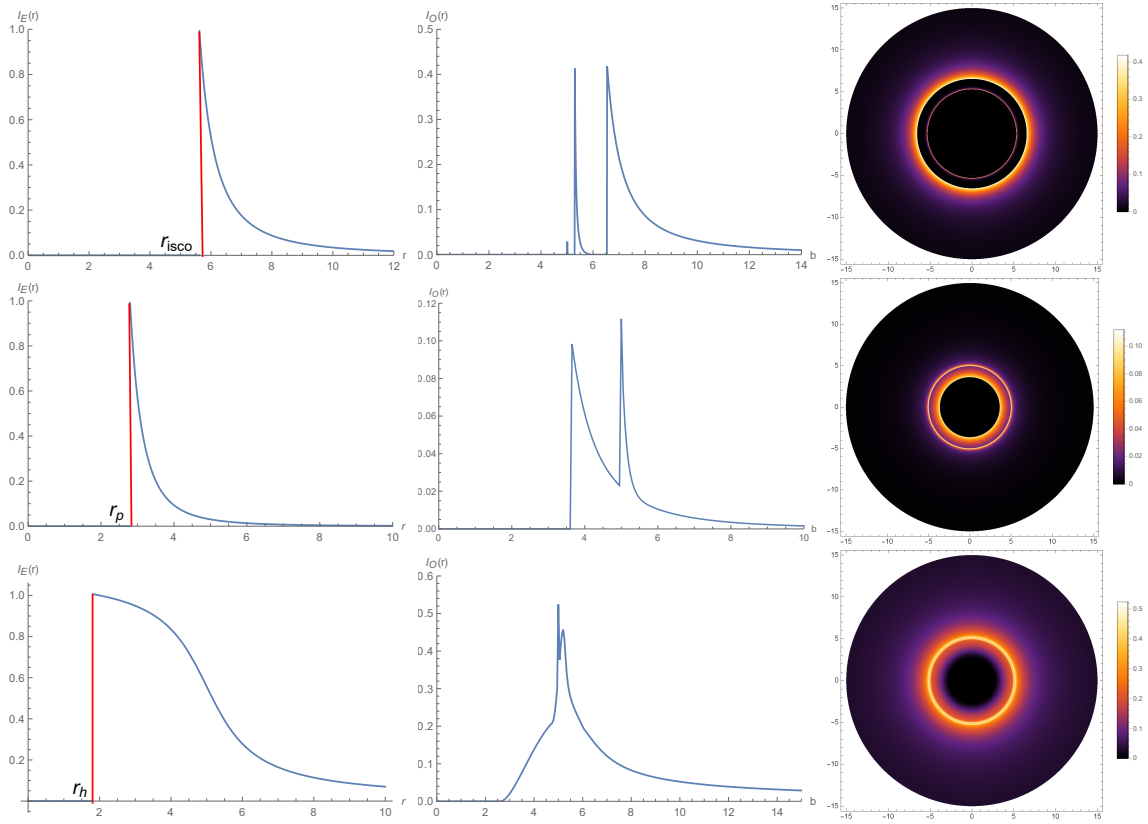


Figure 10. Observational appearance of the thin disk with different emission profiles near the black hole, viewed from a face-on orientation. Here, we set $g = 0.475$ and $M = 1$.

As can be readily seen from Figure 9, for different modes of the emission, both the profile of the black central area and the observation intensity are different. However, the observation intensity obtained by the observer at infinity is mainly provided by the direct emission in all cases. Although the ring can get more brightness from the thin disk, it is highly demagnetized and confined to a narrow region. Therefore, the contribution of the photon ring to the total observed flux is negligible in all cases. In the model where the emission starts at the event horizon, the lens ring has some contribution to the total

observation intensity, but the contribution of the photon ring is still negligible. That is to say, the observation intensity obtained by the distant observer is directly determined by the direct emission. In addition, the contribution of the lens ring to the total observed flux is partially helpful, while that of the photon ring is negligible. The features shown in these images are generally consistent with those in Schwarzschild space-time ($g = 0$) [34]. Then, we also plot the profiles of the emission and observed intensities when $g = 0.7698003$, which is shown in Figure 10. As one can see, there is not much difference in the overall characteristics. However, when the parameter g is changed, the observation intensity, shadow radius and the region bands of lens ring and photon ring are obviously different.

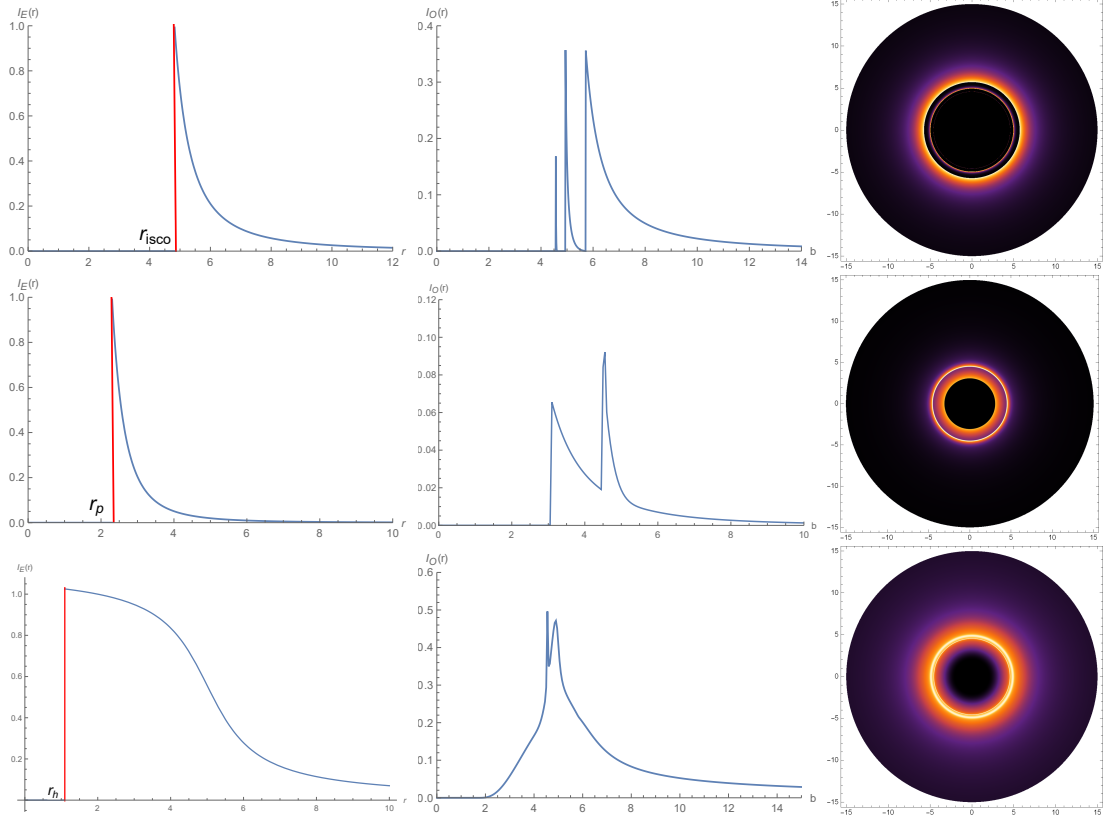


Figure 11. Observational appearance of the thin disk with different emission profiles near the black hole, viewed from a face-on orientation. Here, we set $g = 0.7698003$ and $M = 1$.

5 Conclusions and discussions

It is commonly known that the black hole is surrounded by the accretion matter, and the distribution of accretion plays a key role in the imaging results of black holes. We have investigated the image of a Bardeen black hole and its luminosity under the different accretion models. In particular, we pay close attention to the different image characteristics of the distant observer when the related physical quantities of the black hole changed.

We first studied the shadow and photon sphere of a black hole, surrounded by two different cases of spherically symmetric accretions. For the case of static spherically symmetric accretions, we notice that the observed luminosity increases with the increase of parameter g , although the photon sphere and shadow radius decrease. In addition, the maximum luminosity appears in the region of photon ring, and the central region of the shadow is not completely dark, and the image brightness of the central region increases slightly with the increase of g . For the case of infalling spherical accretion, the observation luminosity is obviously lower than that of the static state, that is, the infalling accretion would have a darker interior than the static one. On the other hand, with the increase of parameter g , the change of observation intensity is more obvious, the observation luminosity at $g = 0.7698003$ is about twice that at $g = 0$ (Schwarzschild black hole). The Doppler effect of the infalling matter leads to the difference between the two kinds of spherical accretion. It must also be mentioned that in both spherical accretion models, there is a great difference in the observed luminosity, but the position of the photon ring and the shadow radii unchanged under the same parameters.

Then, considering the Bardeen black hole surrounded by a geometrically and optically thin disk accretion, we have studied and distinguished the ray trajectories near black holes. For the observer, there is not only a dark central shadow area, but also the photon rings and lens ring in the outer area of the shadow. For different emission modes, the observed luminosity and the range of the observation intensity are different. In addition, although the photon ring accretes through the thin disk more than three times and gains extra brightness, due to the extremely demagnetized, the observer cannot observe the photon rings. Similarly, even the lens ring, due to the high demagnetization, can only provide a very small part of the help for the total observed flux. Therefore, the observed intensities are dominated by direct emission. Obviously, when the relevant physical parameters change, the radius of the black hole shadow, the intensity of observation and the position of photon sphere will change correspondingly. That is, the parameter g not only affects the space-time structure of the black hole, but also plays an important role in the imaging and observation of the Bardeen black hole shadow. Although these results are obtained in the ideal model, it is very important to push forward the theoretical study of black hole shadow as far as possible and lay the foundation for the observation results.

Acknowledgments

This work is supported by the National Natural Science Foundation of China (Grant Nos. 11675140, 11705005, and 11875095).

References

- [1] K. Akiyama *et al.* [Event Horizon Telescope Collaboration], “First M87 Event Horizon Telescope Results. I. The Shadow of the Supermassive Black Hole,” *Astrophys. J.* **875**, no. 1, L1 (2019)
- [2] K. Akiyama *et al.* [Event Horizon Telescope Collaboration], “First M87 Event Horizon Telescope Results. II. Array and Instrumentation,” *Astrophys. J.* **875**, no. 1, L2 (2019)

- [3] K. Akiyama *et al.* [Event Horizon Telescope Collaboration], “First M87 Event Horizon Telescope Results. III. Data Processing and Calibration,” *Astrophys. J.* **875**, no. 1, L3 (2019)
- [4] K. Akiyama *et al.* [Event Horizon Telescope Collaboration], “First M87 Event Horizon Telescope Results. IV. Imaging the Central Supermassive Black Hole,” *Astrophys. J.* **875**, no. 1, L4 (2019)
- [5] K. Akiyama *et al.* [Event Horizon Telescope Collaboration], “First M87 Event Horizon Telescope Results. V. Physical Origin of the Asymmetric Ring,” *Astrophys. J.* **875**, no. 1, L5 (2019)
- [6] K. Akiyama *et al.* [Event Horizon Telescope Collaboration], “First M87 Event Horizon Telescope Results. VI. The Shadow and Mass of the Central Black Hole,” *Astrophys. J.* **875**, no. 1, L6 (2019)
- [7] M. Jaroszynski and A. Kurpiewski, “Optics near kerr black holes: spectra of advection dominated accretion flows,” *Astron. Astrophys.* **326**, 419 (1997)
- [8] R. Shaikh, P. Kocherlakota, R. Narayan and P. S. Joshi, “Shadows of spherically symmetric black holes and naked singularities,” *Mon. Not. Roy. Astron. Soc.* **482** (2019) no.1, 52-64
- [9] S. E. Gralla and A. Lupsasca, “Lensing by Kerr Black Holes,” *Phys. Rev. D* **101**, no. 4, 044031 (2020)
- [10] A. Allahyari, M. Khodadi, S. Vagnozzi and D. F. Mota, “Magnetically charged black holes from non-linear electrodynamics and the Event Horizon Telescope,” *JCAP* **2002**, 003 (2020)
- [11] P. C. Li, M. Guo and B. Chen, “Shadow of a Spinning Black Hole in an Expanding Universe,” *Phys. Rev. D* **101**, no. 8, 084041 (2020)
- [12] I. Banerjee, S. Chakraborty and S. SenGupta, “Silhouette of M87*: A New Window to Peek into the World of Hidden Dimensions,” *Phys. Rev. D* **101**, no. 4, 041301 (2020)
- [13] S. Vagnozzi and L. Visinelli, “Hunting for extra dimensions in the shadow of M87*,” *Phys. Rev. D* **100**, no. 2, 024020 (2019)
- [14] S. Vagnozzi, C. Bambi and L. Visinelli, “Concerns regarding the use of black hole shadows as standard rulers,” *Class. Quant. Grav.* **37**, no. 8, 087001 (2020)
- [15] M. Safarzadeh, A. Loeb and M. Reid, “Constraining a black hole companion for M87* through imaging by the Event Horizon Telescope,” *Mon. Not. Roy. Astron. Soc.* **488**, no. 1, L90 (2019)
- [16] H. Davoudiasl and P. B. Denton, “Ultralight Boson Dark Matter and Event Horizon Telescope Observations of M87*,” *Phys. Rev. Lett.* **123**, no. 2, 021102 (2019)
- [17] R. Roy and U. A. Yajnik, “Evolution of black hole shadow in the presence of ultralight bosons,” *Phys. Lett. B* **803**, 135284 (2020)
- [18] R. Roy and S. Chakrabarti, “A study on black hole shadows in asymptotically de Sitter spacetimes,” *arXiv:2003.14107 [gr-qc]*.
- [19] Y. Chen, J. Shu, X. Xue, Q. Yuan and Y. Zhao, “Probing Axions with Event Horizon Telescope Polarimetric Measurements,” *Phys. Rev. Lett.* **124**, no. 6, 061102 (2020)
- [20] X. Qin, S. Chen and J. Jing, “Image of a regular phantom black hole and its luminosity under spherical accretions,” [*arXiv:2011.04310 [gr-qc]*].
- [21] R. A. Konoplya and A. F. Zinhailo, “Quasinormal modes, stability and shadows of a black hole in the novel 4D Einstein-Gauss-Bonnet gravity,” *arXiv:2003.01188 [gr-qc]*.

- [22] S. U. Islam, R. Kumar and S. G. Ghosh, “Gravitational lensing by black holes in $4D$ Einstein-Gauss-Bonnet gravity,” arXiv:2004.01038 [gr-qc].
- [23] X. H. Jin, Y. X. Gao and D. J. Liu, “Strong gravitational lensing of a 4-dimensional Einstein-Gauss-Bonnet black hole in homogeneous plasma,” arXiv:2004.02261 [gr-qc].
- [24] M. Guo and P. C. Li, “The innermost stable circular orbit and shadow in the novel $4D$ Einstein-Gauss-Bonnet gravity,” arXiv:2003.02523 [gr-qc].
- [25] S. W. Wei and Y. X. Liu, “Testing the nature of Gauss-Bonnet gravity by four-dimensional rotating black hole shadow,” arXiv:2003.07769 [gr-qc].
- [26] A. Grenzebach, V. Perlick and C. Lämmerzahl, “Photon Regions and Shadows of Kerr-Newman-NUT Black Holes with a Cosmological Constant,” *Phys. Rev. D* **89**, no.12, 124004 (2014)
- [27] Q. Li and T. Wang, “Gravitational effect of a plasma on the shadow of Schwarzschild black holes,” [arXiv:2102.00957 [gr-qc]].
- [28] J.-P. Luminet, “Image of a spherical black hole with thin accretion disk,” *Astron. Astrophys.* **75**, 228 (1979).
- [29] P. V. P. Cunha, N. A. Eiró, C. A. R. Herdeiro and J. P. S. Lemos, “Lensing and shadow of a black hole surrounded by a heavy accretion disk,” *JCAP* **2003**, no. 03, 035 (2020)
- [30] R. Narayan, M. D. Johnson and C. F. Gammie, “The Shadow of a Spherically Accreting Black Hole,” *Astrophys. J.* **885**, no. 2, L33 (2019)
- [31] H. Falcke, F. Melia and E. Agol, “Viewing the shadow of the black hole at the galactic center,” *Astrophys. J.* **528**, L13 (2000)
- [32] C. Bambi, “Can the supermassive objects at the centers of galaxies be traversable wormholes? The first test of strong gravity for mm/sub-mm very long baseline interferometry facilities,” *Phys. Rev. D* **87**, 107501 (2013)
- [33] X. X. Zeng, H. Q. Zhang and H. Zhang, “Shadows and photon spheres with spherical accretions in the four-dimensional Gauss–Bonnet black hole,” *Eur. Phys. J. C* **80**, no.9, 872 (2020)
- [34] S. E. Gralla, D. E. Holz and R. M. Wald, “Black Hole Shadows, Photon Rings, and Lensing Rings,” *Phys. Rev. D* **100**, no. 2, 024018 (2019)
- [35] X. X. Zeng and H. Q. Zhang, “Influence of quintessence dark energy on the shadow of black hole,” *Eur. Phys. J. C* **80**, no.11, 1058 (2020)
- [36] J. Peng, M. Guo and X. H. Feng, “Influence of Quantum Correction on the Black Hole Shadows, Photon Rings and Lensing Rings,” [arXiv:2008.00657 [gr-qc]].
- [37] James M Bardeen. Non-singular general-relativistic gravitational collapse. In *Proc. Int. Conf. GR5, Tbilisi*, volume 174, 1968.
- [38] Eloy Ayón-Beato and Alberto Garcia. The Bardeen model as a nonlinear magnetic monopole. *Physics Letters B*, 493(1-2):149–152, 2000.
- [39] Eloy Ayon-Beato and Alberto Garcia. Regular black hole in general relativity coupled to nonlinear electrodynamics. *Physical Review Letters*, 80(23):5056, 1998.
- [40] Sean A Hayward. Formation and evaporation of nonsingular black holes. *Physical Review Letters*, 96(3):031103, 2006.

- [41] Waldemar Berej, Jerzy Matyjasek, Dariusz Tryniecki, and Mariusz Woronowicz. Regular black holes in quadratic gravity. *General Relativity and Gravitation*, 38(5):885–906, 2006.
- [42] A. Borde, “Open and closed universes, initial singularities and inflation,” *Phys. Rev. D* **50**, 3692-3702 (1994)
- [43] A. Borde, “Regular black holes and topology change,” *Phys. Rev. D* **55**, 7615-7617 (1997)
- [44] E. F. Eiroa and C. M. Sendra, “Gravitational lensing by a regular black hole,” *Class. Quant. Grav.* **28**, 085008 (2011)
- [45] P. Pradhan, “Regular Black Holes as Particle Accelerators,” [arXiv:1402.2748 [gr-qc]].
- [46] H. Ghaffarnejad and H. Niad, “Weak Gravitational lensing from regular Bardeen black holes,” *Int. J. Theor. Phys.* **55**, no.3, 1492-1505 (2016)
- [47] M. Saleh, B. B. Thomas and T. C. Kofane, “Thermodynamics and Phase Transition from Regular Bardeen Black Hole Surrounded by Quintessence,” *Int. J. Theor. Phys.* **57**, no.9, 2640-2647 (2018)
- [48] K. V. Rajani, C. L. Ahmed Rizwan, A. Naveena Kumara, D. Vaid and K. M. Ajith, “Regular Bardeen AdS black hole as a heat engine,” *Nucl. Phys. B* **960**, 115166 (2020)
- [49] B. Narzilloev, J. Rayimbaev, S. Shaymatov, A. Abdujabbarov, B. Ahmedov and C. Bambi, *Phys. Rev. D* **102**, no.10, 104062 (2020)
- [50] J. Man and H. Cheng, “The calculation of the thermodynamic quantities of the Bardeen black hole,” *Gen. Rel. Grav.* **46**, 1660 (2014)
- [51] J. L. Synge, “The Escape of Photons from Gravitationally Intense Stars,” *Mon. Not. Roy. Astron. Soc.* **131**, no. 3, 463 (1966).
- [52] J. M. Bardeen, W. H. Press and S. A. Teukolsky, “Rotating black holes: Locally nonrotating frames, energy extraction, and scalar synchrotron radiation,” *Astrophys. J.* **178**, 347 (1972).